J. Plasma Fusion Res. SERIES, Vol.7 (2006) 190-194

X-Ray Spectral Analysis on Electron Interaction with Highly-Charged Ions in Tokyo-EBIT

KATO Daiji, NAKAMURA Nobuyuki[1] and OHTANI Shunsuke[1]

National Institute for Fusion Science, Toki 509-5292, Japan

[1] *University of Electro-Communications, Chofu 182-8585, Japan*

(Received: 14 December 2004 / Accepted: 4 October 2005)

Abstract

Charge state distribution of Xe ions in an electron-beam-ion-trap (EBIT) was studied based on coupled rate equations for ion population density and temperature. A synthetic X-ray spectrum of highly charged Xe ions was compared with an experimental spectrum measured at the Tokyo-EBIT. The observed spectra contain lines from Ne-, Na-, Mg-, Al-, and Si-like ions. Most of those lines have been identified and the wavelengths have been determined experimentally for elements of $Z = 50 - 56$.

Keywords:

highly charged ion, electron beam ion trap, X-ray spectrum

1. Introduction

Development of the electron-beam-ion-traps (EBI Ts) enabled us collision experiments of high-energy electron beam with cold trapped highly charged ions (HCIs). In previous studies at the Tokyo-EBIT [1], we have measured $3l - 2p$ transition wavelengths of Ne-like HCIs for atomic numbers $Z = 50 - 56$ in a X-ray region, and investigated a configuration mixing of the $3l$ excited levels caused by a strong spin-orbit coupling of the 2p-orbital [2,3].

In this work, we analyze satellite lines of lower charge states (Na-like to Si-like) observed near by the Ne-like lines. Charge state abundance of ions in the EBIT does not obey the simple electron collision ionization equilibrium. In the EBIT, axial trapping of the ions is provided by an electrostatic potential well at drift tubes, and radial trapping is provided by a space charge field of the electron beam [4,5]. The ions which gain enough kinetic energies by collision with the electron beam can escape from the trap (evaporation). Charge state distribution is determined by balance between rates at which the various detailed electron-impact ionization, recombination and ion-loss processes take place.

This paper is organized as follows. In Sec. **2**, we compare experimental and synthetic X-ray spectra of Xe ions in the EBIT. Calculations of ion population density and temperature are explained in that section. Identification of unknow satellite lines of the lower charge states for $Z = 50 - 56$ is presented in Sec. **3**. Section **4** is devoted to summarize this work.

Corresponding author's e-mail: kato.daiji@nifs.ac.jp

2. Experimental and synthetic X-ray spectra of Xe HCIs in EBIT

The X-ray transition excited by a 60 μm-diam electron beam was measured at the Tokyo-EBIT with a flat crystal spectrometer [6]. The spectrometer consisted of a flat crystal and a position sensitive proportional counter (PSPC) [1,6] with a backgammon-type cathode. Two types of crystal were used according to objective wavelength; one was LiF(200) with an area of $120 \times 50\,\mathrm{mm}^2$ and another was Si(111) with an area of $120 \times 70\,\mathrm{mm}^2$. The spectrometer was operated in vacuo ($\sim 10^{-7}$ torr) to avoid absorption by air. A beryllium foil with a thickness of 50 μm was used to separate the vacuum of the EBIT ($\sim 10^{-9}$ torr) from that of the spectrometer. Fig. 1 shows an example of the experimental and synthetic X-ray spectra for Xe ions.

The synthetic spectrum was obtained using atomic data of the HULLAC code [7] and a given charge state distribution. The charge state distribution is predicted using a set of coupled rate equations for ion population densities and temperatures,

$$\begin{aligned}
\frac{\mathrm{d}n_q}{\mathrm{d}t} &= \gamma^{\mathrm{EI}}_{q,q-1} n_e n_{q-1} - \left(\gamma^{\mathrm{RR}}_{q-1,q} + \gamma^{\mathrm{EI}}_{q+1,q}\right) n_e n_q \\
&\quad + \gamma^{\mathrm{RR}}_{q,q+1} n_e n_{q+1} - R^{loss}_q n_q, \\
\frac{3}{2}\frac{\mathrm{d}}{\mathrm{d}t}\left(n_q k T_q\right) &= \nu^{e-i}_q n_q \delta E - R^{loss}_q n_q \left(qeV_{ax} + \frac{3}{2} k T_q\right) \\
&\quad + n_q \sum_{q' \neq q} \nu^{\mathrm{i-i}}_{q,q'} \frac{3}{2}\left(k T_{q'} - k T_q\right), \qquad (1)
\end{aligned}$$

© 2006 by The Japan Society of Plasma Science and Nuclear Fusion Research

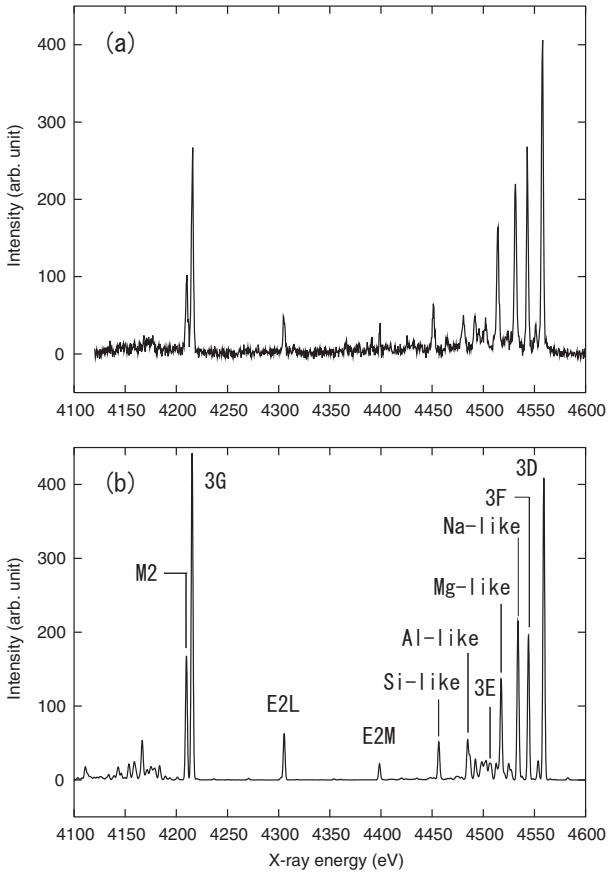

Fig. 1 (a) Experimental X-ray spectrum of Xe ions measured at the Tokyo-EBIT. Electron beam energy $E_e \approx 5540$ eV (below the ionization energy of the Ne-like Xe ion), electric current $I_e \approx 97$ mA, magnetic field strength in the drift tubes $B \approx 4$ T, and axial potential well $V_{ax} \approx 100$ eV. (b) Synthetic spectrum convoluted using the Gaussian distribution function with a full-width-at-half-maximum of 2 eV. 3D, 3E, 3F, 3G, E2M, E2L, and M2 lines are of Ne-like ions.

where n_q and T_q stand for density and temperature for ions of a charge number q, respectively, $\gamma's$ are rate coefficients [$\mathrm{cm^3 s^{-1}}$] for the ion population densities, and $\nu's$ the Coulomb collision frequencies [$\mathrm{s^{-1}}$].

In the right-hand side (RHS) of the first rate equation, four terms are rate of population increase due to electron-impact ionization (EI) of lower charge state $q-1$, depopulation rate due to EI and radiative recombination (RR) of the current charge state q, rate of population increase due to RR of higher charge state $q+1$, and ion-loss rate due to evaporation by electron heating, respectively. The dielectronic recombination (DR) was omitted in the present study. Since energy distribution of the electron beam is narrow, say 50 eV, the DR would contribute only at resonance energies. The ion-loss rate is approximated by a formula for the magnetic-mirror configuration of a uniform magnetic field [8],

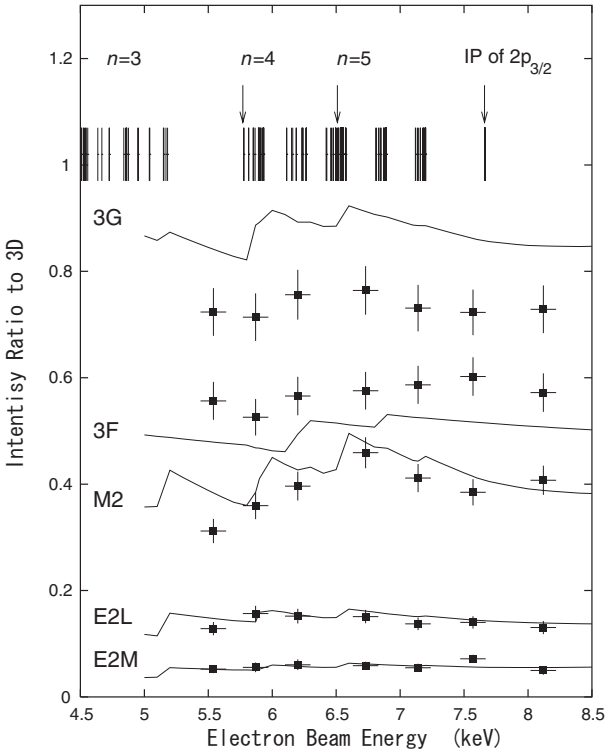

Fig. 2 Intensity variation as a function of electron energy. $2p_{3/2} \rightarrow nl$ excited level energies and the ionization energy of $2p_{3/2}$ orbital are indicated by vertical lines in the upper part of the figure.

$$R_q^{\mathrm{loss}} \approx \frac{2}{0.922\sqrt{\pi}} \frac{\exp[-\omega]}{\omega} \gamma_{q,q}^{\mathrm{i-i}}, \qquad (2)$$

where $\omega = qeV_{ax}/kT_q$, and qeV_{ax} is the axial potential barrier. In the RHS of the second rate equation, the first term represents the electron heating of trapped ions, the second term evaporative cooling, and the third term thermal energy exchange. $\delta E = 2\frac{m_e}{m_i}E_e$ is energy gain by single electron-collision at electron energy E_e provided $E_e > \frac{3}{2}kT_q$, where $m_{e,i}$ are electron and ion masses, respectively.

In the present calculation, we assumed that neutral Xe gas was injected continuously into the trap so that the neutral density was maintained at $10^5\,\mathrm{cm^{-3}}$. At the experimental condition (see caption of Fig. 1 (a)), the population densities for $q = 40, 41, 42, 43, 44$ were obtained to be $n_q \approx 0.25, 0.38, 0.67, 1.1, 2.1 \times 10^9\,\mathrm{cm^{-3}}$, respectively, and the ion temperature $kT_q \approx 800$ eV for all the $q = 40-44$. Charge exchange (CX) with the neutral Xe atoms may affect the charge state distribution to some extent. However, it was neglected in the present calculations, since the CX rate was estimated to be several orders of magnitudes smaller than the ion-loss rate for the neutral density of $10^5\,\mathrm{cm^{-3}}$ [9].

In Fig. 1 (b), four electric-dipole lines of the Ne-like ions are indicated as 3D, 3E, 3F, and 3G. Their upper levels are $(2p_{3/2}^{-1}3d_{5/2})_{J=1}$, $(2p_{3/2}^{-1}3d_{3/2})_{J=1}$,

Table 1 Wavelengths of $n=3$ to 2 transitions in highly charged Sn, Sb, Te, I, Xe, Cs and Ba ions. The lower levels of the transitions are the ground state for all the lines. All values are given in Å. The numbers in the parentheses represent the experimental uncertainties, e.g. 3.3540 (4) represents 3.3540 ± 0.0004. Key notations by Loulergue and Nussbaumer [10] and Beiersdorfer *et al.* [11] are used. [a] Beiersdorfer *et al.* [12,13]; [b] present; [c] Beiersdorfer *et al.* [11].

Element (Z)	Charge state	Upper level	Key	λ_{expt}	Reference lines
Sn (50)	Ne	$(2p_{3/2}^{-1}3p_{3/2})_2$	E2M	3.3540(4)	[a] Ar^{16+} K-β_1, K-δ_1
	Ne	$(2p_{1/2}^{-1}3s)_1$	3F	3.2764(3)	[a] Ar^{16+} K-β_1, K-δ_1
	Ne	$(2p_{3/2}^{-1}3d_{3/2})_1$	3E	3.2695(4)	[b] Sn^{40+} 3D, 3F
	Mg	$(2p_{3/2}^{-1}3s^2 3d_{5/2})_1$		3.2673(3)	[b] Sn^{40+} 3D, 3F
	Na	$(2p_{3/2}^{-1}3s3d_{5/2})_{3/2}$		3.2514(4)	[a] Ar^{16+} K-β_1, K-δ_1
	Na	$(2p_{3/2}^{-1}3s3d_{5/2})_{1/2}$		3.2416(4)	[a] Ar^{16+} K-β_1, K-δ_1
	Ne	$(2p_{3/2}^{-1}3d_{5/2})_1$	3D	3.2326(4)	[a] Ar^{16+} K-β_1, K-δ_1
	Ne	$(2p_{1/2}^{-1}3p_{3/2})_2$	E2U	3.1547(5)	[a] Ar^{16+} K-β_1, K-δ_1
	Mg	$(2p_{1/2}^{-1}3s^2 3d_{3/2})_1$		3.0931(5)	[a] Ar^{16+} K-β_1, K-δ_1
	Na	$(2p_{1/2}^{-1}3s3d_{3/2})_{3/2}$		3.0823(5)	[a] Ar^{16+} K-β_1, K-δ_1
Sb (51)	Ne	$(2p_{3/2}^{-1}3d_{3/2})_1$	3E	3.1287(2)	[a] Ar^{16+} K-δ_1, K-ϵ_1
	Ne	$(2p_{1/2}^{-1}3s)_1$	3F	3.1253(1)	[a] Ar^{16+} K-δ_1, K-ϵ_1
	Mg	$(2p_{3/2}^{-1}3s^2 3d_{5/2})_1$		3.1239(2)	[a] Ar^{16+} K-δ_1, K-ϵ_1
	Na	$(2p_{3/2}^{-1}3s3d_{5/2})_{3/2}$		3.1103(1)	[a] Ar^{16+} K-δ_1, K-ϵ_1
	Na	$(2p_{3/2}^{-1}3s3d_{5/2})_{1/2}$		3.1005(2)	[a] Ar^{16+} K-δ_1, K-ϵ_1
	Ne	$(2p_{3/2}^{-1}3d_{5/2})_1$	3D	3.0926(2)	[a] Ar^{16+} K-δ_1, K-ϵ_1
Te (52)	Ne	$(2p_{3/2}^{-1}3d_{3/2})_1$	3E	2.9954(4)	[c] Xe^{44+} M2, E2L
	Mg	$(2p_{3/2}^{-1}3s^2 3d_{5/2})_1$		2.9902(3)	[c] Xe^{44+} M2, E2L
	Ne	$(2p_{1/2}^{-1}3s)_1$	3F	2.9844(3)	[c] Xe^{44+} M2, E2L
	Na	$(2p_{3/2}^{-1}3s3d_{5/2})_{3/2}$		2.9775(3)	[c] Xe^{44+} M2, E2L
	Ne	$(2p_{3/2}^{-1}3d_{5/2})_1$	3D	2.9608(2)	[c] Xe^{44+} M2, E2L
	Ne	$(2p_{1/2}^{-1}3p_{3/2})_2$	E2U	2.8712(3)	[c] Xe^{44+} M2, E2L
I (53)	Si	$(2p_{3/2}^{-1}3s^2 3p_{1/2}^2 3d_{5/2})_1$		2.9057(3)	[c] Xe^{44+} E2L, E2M
	Mg	$(2p_{3/2}^{-1}3s^2 3d_{5/2})_1$		2.8640(2)	[c] Xe^{44+} E2L, E2M
	Ne	$(2p_{1/2}^{-1}3s)_1$	3F	2.8524(2)	[c] Xe^{44+} E2L, E2M
	Na	$(2p_{3/2}^{-1}3s3d_{5/2})_{3/2}$		2.8524(2)	[c] Xe^{44+} E2L, E2M
	Ne	$(2p_{3/2}^{-1}3d_{5/2})_1$	3D	2.8370(2)	[c] Xe^{44+} E2L, E2M
Xe (54)	Si	$(2p_{3/2}^{-1}3s^2 3p_{1/2}^2 3d_{5/2})_1$		2.7849(2)	[c] Xe^{44+} E2M, 3F
	Al	$(2p_{3/2}^{-1}3s^2 3p_{1/2}3d_{5/2})_{3/2+1/2}$		2.7665(2)	[c] Xe^{44+} E2M, 3F
	Mg	$(2p_{3/2}^{-1}3s3p_{3/2}^2)_1$		2.7596(2)	[c] Xe^{44+} E2M, 3F
	Ne	$(2p_{3/2}^{-1}3d_{3/2})_1$	3E	2.7535(2)	[c] Xe^{44+} E2M, 3F
	Mg	$(2p_{3/2}^{-1}3s^2 3d_{5/2})_1$		2.7460(2)	[c] Xe^{44+} E2M, 3F
	Na	$(2p_{3/2}^{-1}3s3d_{5/2})_{3/2}$		2.7358(2)	[c] Xe^{44+} E2M, 3F
	Mg	$(2p_{1/2}^{-1}3s^2 3d_{3/2})_1$		2.5764(3)	[c] Xe^{44+} E2U, 3C
	Na	$(2p_{1/2}^{-1}3s3d_{3/2})_1$		2.5674(3)	[c] Xe^{44+} E2U, 3C
Cs (55)	Ne	$(2p_{3/2}^{-1}3d_{3/2})_1$	3E	2.6427(4)	[c] Xe^{44+} E2U, 3C
	Na	$(2p_{3/2}^{-1}3s3d_{5/2})_{3/2}$		2.6256(4)	[c] Xe^{44+} E2U, 3C
	Ne	$(2p_{3/2}^{-1}3d_{5/2})_1$	3D	2.6149(3)	[c] Xe^{44+} E2U, 3C
	Ne	$(2p_{1/2}^{-1}3s)_1$	3F	2.6076(3)	[c] Xe^{44+} E2U, 3C
Ba (56)	Ne	$(2p_{3/2}^{-1}3p_{1/2})_2$	E2L	2.6588(5)	[c] Xe^{44+} E2U, 3C
	Ne	$(2p_{3/2}^{-1}3p_{3/2})_2$	E2M	2.5976(3)	[c] Xe^{44+} E2U, 3C
	Ne	$(2p_{3/2}^{-1}3d_{3/2})_1$	3E	2.5398(3)	[c] Xe^{44+} 3C, 3B
	Na	$(2p_{3/2}^{-1}3s3d_{5/2})_{3/2}$		2.5225(3)	[c] Xe^{44+} 3C, 3B
	Ne	$(2p_{3/2}^{-1}3d_{5/2})_1$	3D	2.5111(3)	[c] Xe^{44+} 3C, 3B
	Ne	$(2p_{1/2}^{-1}3s)_1$	3F	2.4995(3)	[c] Xe^{44+} 3B, 3A

$(2p_{1/2}^{-1}3s)_{J=1}$, and $(2p_{3/2}^{-1}3s)_{J=1}$, respectively. Two electric-quadruple lines E2M and E2L and one magnetic-quadruple line M2 have upper levels of $(2p_{3/2}^{-1}3p_{1/2})_{J=2}$, $(2p_{3/2}^{-1}3p_{1/2})_{J=2}$, and $(2p_{3/2}^{-1}3s)_{J=2}$, respectively. Lower levels for those lines are of the ground state $(2p^6)_{J=0}$. As in the figure, relative intensities of the satellite lines obtained using the calculated charge state distribution agree with the experimental measurements. However, significant discrepancies between the synthetic spectrum and the experimental spectrum remain for intensity ratios of Ne-like 3F and 3G lines to the 3D line. Fig. 2 compares experimental measurements and theoretical predictions for the line intensity ratios as a function of the electron beam energy. Sawtooth profiles of the intensity variation are due to cascade feeding from higher excited levels. The discrepancies are apparent for the 3F and 3G lines, while good agreement is obtained for other Ne-like lines.

3. Identification of satellite lines

Satellite lines of lower charge states (Na-like to Si-like) were observed near by the Ne-like lines. Wavelengths of the satellite lines for $Z = 50 - 56$ were experimentally determined as listed in Table 1. Reference lines which were used for each line are also listed in the table. The observations for Sn were done with both LiF(200) and Si(111) to obtain two spectra which differed in dispersion. At first, a spectrum with wide bandwidth (small dispersion) was observed with Si(111) so that the two reference lines, K-α and K-δ of He-like Ar, appeared in the same spectral range. From this spectrum the wavelengths of all the lines except 3E and $(2p_{3/2}^{-1}3s^23d_{5/2})_1 \rightarrow 2p^63s^2$ were determined. The second spectrum with narrow bandwidth (large dispersion) was obtained with LiF(200) so that 3E and $(2p_{3/2}^{-1}3s^23d_{5/2})_1 \rightarrow 2p^63s^2$ could be resolved. The wavelengths of those lines were then determined by using the wavelengths of 3D and 3F determined from the wide bandwidth spectrum as references. Uncertainties in the experimental wavelengths were estimated from the quadrature sum of three contributions: the uncertainty in the peak position of the reference lines, that of objective line, and the uncertainties in the reference wavelengths. The uncertainty in the peak position includes the statistical error and the error arising from the calibration procedure.

The identification of the lines was done by comparing the measured spectra carefully with the synthetic spectra. For the Na-like and Mg-like ions, some lines were identified as two-electron-one-photon transitions. Although a two-electron-one-photon transitions is usually very weak, it becomes possible when the upper state has strong configuration interaction with the state which can decay via fast electric-dipole transitions. An example is $(2p_{3/2}^{-1}3p_{3/2}^2)_{J=1/2} \rightarrow 2p^63s$ in the Na-like system. In this Z-region, $(2p_{3/2}^{-1}3p^2)_{J=1/2}$ has strong configuration interaction with $(2p_{3/2}^{-1}3s3d_{5/2})_{J=1/2}$, which can rapidly decay to the ground state $2p^63s$. The two-electron-one-photon transitions thus occur with relatively strong intensity in this Z-region. The same situation can also be found in the Mg-like system; the two-electron-one-photon transition, $(2p_{3/2}^{-1}3s3p_{3/2}^2)_{J=1} \rightarrow 2p^63s^2$, become possible due to the strong configuration interaction between $(2p_{3/2}^{-1}3s3p_{3/2}^2)_{J=1}$ and $(2p_{3/2}^{-1}3s^23d_{5/2})_{J=1}$.

4. Summary

We measured $n = 3$ to 2 transitions in highly charged ions with $Z = 50$ to 56 in near Ne-like charge states. Comparing the experimental spectra with the synthetic spectra, most of the spectral lines have been identified and the corresponding wavelengths were experimentally determined. Discrepancies between the experimental spectrum and the synthetic spectrum remain for the line intensities of the 3F and 3G. It is noted that we have omitted the polarization effect of line emission, whereas the present experimental spectrum was measured at the right angle to the electron beam. If electron impact excitation makes different alignment of magnetic sub-levels for each excited state, the omission of the polarization effect would cause error in the line intensity ratios of the synthetic spectrum. We leave investigation of the polarization effect in future studies. The effects of strong configuration interactions have been found as the two-electron-one-photon transition in the Na-like and Mg-like ions.

We owe it to collaborations with JAERI that the HULLAC code was available for this work. D. K. wish to thank Dr. Yu. Ralchenko and Prof. U. I. Safronova for comments on this work.

References

[1] N. Nakamura, D. Kato and S. Ohtani, Phys. Rev. A **61**, 052510 (2000).

[2] T. Kagawa, Y. Honda and S. Kiyokawa, Phys. Rev. A **44**, 7092 (1991).

[3] D. Kato *et al.*, Phys. Scr. **T92**, 126 (2001).

[4] F.J. Currell *et al.*, J. Phys. Soc. Jpn. **65**, 3186 (1996).

[5] H. Watanabe *et al.*, J. Phys. Soc. Jpn. **66**, 3795 (1997).

[6] N. Nakamura, Rev. Sci. Instrum. **71**, 4065 (2000).

[7] A. Bar-Shalom *et al.*, *The HULLAC Package*

Computer Set of Codes for Atomic Structure and Processes in Plasmas, unpublished.

[8] R.E. Marrs, Nucl. Instrum. Methods Phys. Res. B **149**, 182 (1999).

[9] B.M. Penetrante *et al.*, Phys. Rev. A **43**, 4861 (1991).

[10] M. Loulergue and H. Nussbaumer, Astron. Astrophys. **45**, 125 (1975).

[11] P. Beiersdorfer *et al.*, Phys. Rev. A **37**, 4153 (1988).

[12] P. Beiersdorfer *et al.*, Phys. Rev. A **40**, 150 (1989).

[13] P. Beiersdorfer *et al.*, Phys. Rev. A **52**, 2693 (1995).